An experimental and kinetic modeling study of 3-methyl-2-butenol (prenol) oxidation

Nitin Lokachari[1], Scott W. Wagnon[2,*], Goutham Kukkadapu[2], William J. Pitz[2], Henry J. Curran[1]

[1]Combustion Chemistry Centre, School of Chemistry, Ryan Institute, MaREI, National University of Ireland Galway, Galway, H91 TK33, Ireland

[2]Lawrence Livermore National Laboratory, Livermore, CA 94551, USA

*Corresponding author : wagnon1@llnl.gov

Abstract

Longer chain alcohols with four to five carbon atoms are attractive alternative fuels as they can be derived from biological sources and their combustion leads to lower exhaust gas levels of NO_x and soot compared to commercial fossil fuels. The auto-ignition behavior of fuels that contain both a hydroxyl group and a C=C double bond in their molecular structure are not well established in the literature. Understanding the influence of these functional groups on the ignition behavior of fuels is critical in the development of tailor-made fuels for advanced combustion engines. In this study, ignition delay times of an unsaturated alcohol, 3-methyl-2-butenol (prenol) in air are measured using a high-pressure shock tube and a rapid compression machine at pressures of 15 and 30 bar at equivalence ratios of 0.5, 1.0 and 2.0 in 'air' in the temperature range 600 – 1400 K. A detailed kinetic model is developed and validated using the new experimental data in this study. In addition, speciation data in a jet-stirred reactor, ignition delay times and laminar burning velocities available in the literature were also used to validate the new kinetic model. Fuel flux and sensitivity analyses are performed using this new model to determine the important fuel consumption pathways and critical reactions that affect the reactivity of prenol.

Keywords: Prenol, rapid compression time, kinetic modeling, ignition delay time, shock tube

1. Introduction

One of the biggest limitations to improving the thermal efficiency of spark ignition (SI) engines is the knock tendency of fuels, which limits engines from operating at high compression ratios. Engine knock arises from the auto-ignition of a portion of the fuel mixture ahead of the propagating flame. The higher the octane number the more resistant a fuel is to autoignition. To reflect the knock resistance of fuels in SI engines, the research octane number (RON) and the motor octane number (MON) scales are adopted as the limiting operating conditions for gasoline fuels in engines.[1] Both the RON and MON scales are based on alkanes; *iso*-octane is assigned a value of 100 and *n*-heptane a value of 0, which define two extremes in reactivity. With advances in the development of engine combustion systems, such as homogenous charge compression ignition (HCCI) or other strategies that can adapt to a variety of fuels, the use of biofuels as alternative fuels or fuel additives is possible.[2, 3] A fuel's octane number can be enhanced by blending antiknock additives, such as oxygenates to the base fuel.[4] In addition to an increase in transportation fuel use, shifting demand between gasoline and diesel, and increasingly stringent emissions standards are motivating fuel suppliers to look for new blendstock options that can provide performance advantages and market benefits. A large number of potential blendstocks remain unused, as they lack a comprehensive collection of fuel properties and engine-performance data required to assess their potential.[5] Alcohols containing four to five carbon atoms are one such chemical family that can increase major fuel properties such as RON and octane sensitivity (OS = RON – MON). Furthermore, adding alcohols to the combustion chamber can also increase the time for end-gas auto-ignition.[6]

The U.S. Department of Energy (DOE) Co-Optimization of Fuels and Engines (Co-Optima) initiative is focused on understanding how new high-performance sustainable fuels

can boost engine efficiency and cut emissions when combined with advanced combustion engines. The opportunity exists to discover promising fuels which possess properties, such as RON and OS, that improve engine performance by enhancing a fuel's resistance to autoignition while operating at high compression ratios. This study focuses on one such fuel candidate, which is an unsaturated alcohol, 3-methyl-2-butenol, commonly known as prenol. One of the criteria in the Co-Optima blendstock selection process for boosted SI gasoline engines was to consider fuels with RON values greater than 98.[5, 7] However, prenol (RON = 93.5) was still considered as it exhibits a significantly higher RON when blended with gasoline blendstocks. Prenol has the unusual property of increasing the RON of the mixture to a higher value than either the blendstocks for oxygenated blending (BOB) or neat prenol, which was reported recently by Monroe et al.[8]. They referred to this phenomenon as 'octane hyperboosting' to distinguish it from more commonly observed synergistic blending of oxygenates to gasoline, in which the RON of the mixture lies between the RON of the individual components.

Several studies illustrate the potential for renewable bio-synthetic production of prenol. Conventionally manufactured from petroleum-derived isobutene and formaldehyde, prenol is not naturally a high yield by-product of organisms.[9] Zheng et al.[9] presented a promising strategy for high-specificity production of prenol from renewable sugar in a microbial fermentation process. In addition, prenol and other C_5 alcohols have recently been shown to be formed from microbial production pathways in engineered *Escherichia coli* strains.[10-12] Further studies are required to determine if such processes scale successfully from benchtops to industrial facilities.

Despite growing interest in prenol as a transportation fuel, fundamental combustion studies of autoignition, laminar burning velocity (LBV), or intermediate species and chemical kinetic models are currently limited in the literature. Ninnemann et al.[13] presented

experimental ignition delay time (IDT) and LBV measurements of prenol and iso-prenol (3-methyl-3-butenol). Ninnemann et al. highlighted the need for experiments at relatively lower temperatures and higher pressures for a wider validation of prenol model. De Bruycker et al.[14] measured species concentration profiles of prenol and iso-prenol at different oxidation and pyrolysis conditions and further developed a kinetic model using Genesys.[15] This current study focuses on experimental and kinetic modeling investigations on the autoignition characteristics of prenol over a wide range of engine relevant conditions together with further validation of the newly developed model using the existing literature data.

This paper is organized by first providing a brief overview of the experimental methodologies in Section 2, followed by a detailed description of our kinetic modeling of prenol chemistry in Section 3. A discussion of the important findings from this study and model validation using the data available in the literature follows in Section 4 and a summary along with recommendations for future work are presented in Section 5.

2. Experimental facilities

Prenol (99%) was obtained from Sigma-Aldrich, while O_2 (99.99%), N_2 (99.99%) and helium (He) (99.97%) were supplied by BOC Ireland. The experimental conditions investigated are listed in Table 1. High temperature (900 – 1400 K) IDTs for the prenol/"air" mixtures were measured behind reflected shock waves in a high-pressure shock-tube (HPST) facility, where the auto-ignition time scales ranged from 0.03 – 2.5 ms and relatively slower IDTs in the range of 5 – 300 ms in the low temperature (600 – 900 K) were measured in a rapid compression machine (RCM). To prepare the fuel-air mixtures, prenol, O_2 and N_2 were added in the order of increasing partial pressure and the temperature of the mixing tank and the system manifold were maintained at 60 °C to prevent fuel condensation. The partial pressures of the fuel mixtures were maintained at a pressure of at least a factor of three below their corresponding saturation vapor pressure at a given temperature. Fuel mixtures were

diffusively mixed for at least 6 – 8 h to achieve homogeneity. Detailed descriptions of these two NUI Galway facilities and their experimental operation have previously been reported[16, 17] and are only briefly discussed here.

Table 1. Experimental conditions of the prenol/O_2/diluent mole fraction compositions investigated in this study at p_C = 15 and 30 bar, T_C = 600 – 1400 K in both the HPST and RCM.

φ	**Prenol**	**O_2**	**N_2**
0.5	0.0148	0.2069	0.7783
1.0	0.0291	0.2039	0.7670
2.0	0.0566	0.1981	0.7453

2.1 High pressure shock tube (NUIG): The facility is a 9 m long stainless-steel tube with uniform cross-section of 63.5 mm internal diameter, divided into a driver section (3 m), a driven section (5.7 m) and a double-diaphragm section. The 30 cm double-diaphragm section separates the tube into two sections and enables improved control of the shock wave generated. To perform an experiment all sections are evacuated to approximately 0.01 bar, with the driven section charged with the test gas. Helium, used as the driver gas, is fed into both the high-pressure (driver) and diaphragm sections. When the double-diaphragm section is evacuated and the diaphragm bursts, the pressure difference between the driver and driven sections results in the formation of a shock wave, formed by expansion of the driver gas, which propagates at supersonic speeds through the driven section, rapidly compressing and heating the test gas (almost instantaneously) to the desired thermodynamic conditions at the end-wall before auto-ignition.

The incident shock velocity at the end-wall was calculated by extrapolating the linear velocity equation calculated using six pressure transducers (PCB 113B24) mounted at different positions in the side-wall of the driven section. The compressed pressure and temperature conditions are calculated using the “reflected shock” routine in Gaseq[18]. The IDT

is defined as the time interval between the pressure rise due to the arrival of the shock wave at the end-wall and the pressure rise due to ignition event. This is measured using a dynamic Kistler 603B pressure transducer placed at the centre of the end-wall. For this study, the error for the measured pressures behind the reflected shock wave was limited to 1%. The uncertainty in the reflected shock temperature (T_5) is mainly attributed to the uncertainty of the incident shock velocity (*Vs*) measurement, which is further determined by the uncertainties in the precise positions of the pressure transducers and the shock pass time recorded by the signal relayed to the oscilloscope from the pressure transducers.[19] The average uncertainties in T_5 and in the IDT measurements using the NUIG HPST are $\pm 15 - 20$ K and ~20% in the temperature range $1000 - 1500$ K. More details regarding the uncertainty measurements in the NUIG facilities have already been published.[20]

2.2 Rapid compression machine (NUIG): The RCM facility has a 38 mm bore and 168 mm stroke and employs an opposed twin-piston arrangement with each piston attached to a connecting rod with a pneumatic driver piston on the opposite end and a hydraulic piston in-between. The creviced pistons, that largely limit the turbulence/roll-up vortices generated in the test gas, are pneumatically driven, and mechanically locked at the end of compression.[21] RCM experiments are actuated by fully retracting the pistons and pressurizing the hydraulic chamber to 40 bar using hydraulic oil. Once the pistons are locked the pressure drops due to heat losses to the surroundings. To account for this heat loss effect in simulating these experiments, non-reactive pressure histories are recorded for every experimental condition, in which identical mixtures are prepared but O_2 is replaced by N_2. To determine the compressed gas temperature, the initial temperature, pressure, mixture composition and compressed gas pressure of each experiment are used using the "adiabatic compression/expansion" routine in Gaseq.[18] A Kistler 6045B piezoelectric pressure transducer, mounted on the side wall of reaction chamber, enables time-resolved measurements of heat losses and IDT. The

uncertainties in T_C and IDT measurements are in the range of ± 5 – 15 K and ± 20 – 25%, respectively, in the temperature range 600 – 900 K.[20]

3. Chemical kinetic modeling

The chemistry of alcohols and alkenes relevant to autoignition in an engine has characteristic features. Prenol combines the characteristics of both alcohols (ȮH moiety) and alkenes (C=C double bond). The presence of these functional groups aid the scavenging of reactive ȮH and $HȮ_2$ radicals by promoting abstraction of the relatively weaker hydrogen atoms i.e., allylic H-atoms and the alpha H-atoms next to the ȮH moiety.[22] These abstractions lead to the formation of relatively unreactive allylic radicals. In particular, the α-hydroxy radicals formed can quickly react with molecular oxygen to form an aldehyde and an $HȮ_2$ radical.[23] Also, the double bond in prenol allows the addition of ȮH and $HȮ_2$ radicals which leads to an adduct that is less reactive than typical low temperature branching products.

AramcoMech2.0[24] was adopted as the base chemistry in this work which includes C_0 – C_4 kinetics and the C_5 species chemistry includes contributions from Sarathy et al.[22] The description of the kinetic model development here will mainly focus on the key reaction classes of prenol. Since there are limited experimental and theoretical rate coefficients available for prenol and its intermediates that contain ȮH and double bond moieties, almost of the rate coefficient information discussed below are taken from similar reactions occurring in alcohols or alkenes. Examples are given below of reactions that are analogous to those in prenol and its intermediates and are used to derive rate coefficients. When the specific analogy is not given, the reader is referred to the well annotated kinetic mechanism in supplementary data. In this study, the thermochemical data have been calculated for all of the species that are of interest to prenol oxidation using Benson's group additivity method in THERM software[25] based on the group values from recent publications.[26, 27]

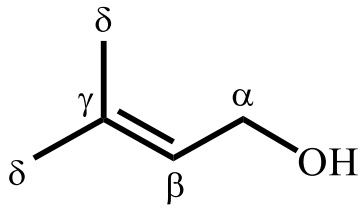

Figure 1: A two-dimensional representation of prenol (3-methyl-2-butenol) with carbon sites labelled.

The chemical kinetic mechanism, thermodynamic data, transport data, and species dictionary are included as supplemental data. Throughout much of the manuscript, model names are used, and readers are encouraged to use the species dictionary for interpretation which contains a SMILES and InChI for each species.

3.1 Pyrolytic reactions: Unimolecular decomposition reactions involving C_γ–C_δ and C_δ–H bond cleavage (see Fig. 1 definition of carbon sites in prenol) were included assuming analogous pressure dependent rate coefficients, multiplied by a factor of two for the reaction path degeneracy of prenol, calculated at the CCSD(T)/cc-pVTZ level of theory for propene by Ye et al.[28] Additional decomposition pathways in prenol via breakage of C_α–C_β and C–O bonds were implemented from Tsang et al.[29, 30] using analogous rate coefficients for 1-butene and allyl alcohol. The six-membered unimolecular water elimination reaction via an allylic H-atom shift resulting in the formation of isoprene and H_2O is included by adopting the calculations of De Bruycker et al.[14] at the CBS-QB3 level of theory.

3.2 H-atom abstraction reactions: Prenol has ten hydrogen atoms; six are primary allylic H-atoms, one secondary vinylic H-atom at the β carbon, two secondary allylic H-atoms at the α site, and one in the hydroxyl moiety (Fig. 1). At low and intermediate temperatures (600 – 1200 K) the most important radicals abstracting hydrogen atoms are $\dot{O}H$ and $H\dot{O}_2$ radicals whereas $\dot{H}$ atoms and $\dot{C}H_3$ radicals become important at higher temperatures (> 1200 K).

Table 2 lists the rate coefficients adopted from various studies for a variety of H-atom abstractors. The rate coefficients were adopted either from computational calculations or estimated as listed in Table 2, due to the lack of direct measurements for this reaction class at the conditions of interest to this study.

Table 2. List of hydrogen abstraction reactions and associated literature.

H-abstraction site/radical formed[1]	**Radical**	**Ref.**	**Comment**
Primary allylic site ($a\dot{C}_5H_8$-dOH-c) SMILES: C=C(C)[CH]CO	O_2	31	iC_4H_8 analogy
	$\dot{H}$ and $\dot{C}H_3$	14	CBS-QB3
	Ö	32	A×2, for twice the equivalent $\dot{C}H_3$ in prenol compared to propene
	ȮH		Private communication with Mohamed et al. [33]
	$H\dot{O}_2$	34	A×2, for twice the equivalent $\dot{C}H_3$ in prenol compared to propene
Alpha hydrogen site ($b\dot{C}_5H_8$dj-dOH) SMILES: OC=C[C](C)C	O_2	35	Estimate
	$\dot{H}$ and $\dot{C}H_3$	14	CBS-QB3
	Ö	32	A/1.5, as prenol contains 2 alpha C–H and compared to 3 C–H in the propene analogy; Ea-2 kcal/mol, reflecting a weaker BDE for the alpha C–H in prenol
	ȮH		Private communication with Mohamed et al.[33]
	$H\dot{O}_2$	14	CBS-QB3

ȮH moiety (b2e3M1Ȯj) SMILES: CC(C)=CC[O]	O_2	35	Estimate
	Ḣ and $\dot{C}H_3$	14	CBS-QB3
	Ö	36	Ethanol analogy
	ȮH		Private communication with Mohamed et al.[33]
	$H\dot{O}_2$	37	Ethanol analogy

[1] See Fig. 1 for definition of sites α, β, γ, δ. See supplementary material for species name definitions.

3.3 Unimolecular reactions of prenol radicals: The hydroxy-alkenyl radical ($a\dot{C}_5H_8$-dOH-c) can undergo β-scission forming a C_5 di-enol and a Ḣ atom (R1) or isoprene and an ȮH radical (R2). The rate coefficients for R1 and R2 were adopted from calculations by Li et al.[38] for but-1-en-3-yl to 1,3 butadiene + Ḣ and De Bruycker et al.,[14] respectively. The β-scission reactions of α-hydroxy-alkenyl ($b\dot{C}_5H_8$dj-dOH) radicals (R3) and alkoxy (b2e3M1Ȯj) radicals (R4) were taken from De Bruycker et al.[14] and Goldsmith et al.[39] for allyloxy ($C_3H_5\dot{O}$) respectively. The isomerization reaction rate coefficients of $a\dot{C}_5H_8$-dOH-c to form $b\dot{C}_5H_8$dj-dOH (R5) and b2e3M1Ȯj (R6) were taken from De Bruycker et al.[14] and estimated as a primary to primary 1,5 H-shift using the approach of Matheu et al.,[40] respectively.

Table 3. List of unimolecular reactions of prenol radicals and their respective analogies.

Reaction	Analogous reaction	
$a\dot{C}_5H_8$-dOH-c = aCC_5H_7-dOH + $\dot{H}$	$\dot{C}_4H_7$1-3 = C_4H_6 + $\dot{H}$	R1
b13de2m + $\dot{O}H$ = $a\dot{C}_5H_8$-dOH-c	N/A	R2
$b\dot{C}_5H_8$dj-dOH = iC_5D2Y4 + $\dot{H}$	N/A	R3
b2e3m1$\dot{O}$j = $i\dot{C}_4H_7$-i1 + CH_2O	$C_3H_5\dot{O}$ = $\dot{C}_2H_3$ + CH_2O	R4
$b\dot{C}_5H_8$dj-dOH = $a\dot{C}_5H_8$-dOH-c	N/A	R5
b2e3m1$\dot{O}$j = $a\dot{C}_5H_8$-dOH-c	$CH_3RRR\dot{C}H_2$ = $\dot{C}H_2RRRCH_3$	R6

3.4 Reactions of O_2 and $H\dot{O}_2$ with prenol radicals: At low to intermediate temperatures $a\dot{C}_5H_8$-dOH-c and $b\dot{C}_5H_8$dj-dOH radicals react with O_2 and $H\dot{O}_2$ radicals enhancing the low temperature reactivity of the system. This subset of reactions were modeled by adopting analogies to reactions involving 2-methyl-allyl ($i\dot{C}_4H_7$) and allyl ($\dot{C}_3H_5$-a) radicals from Chen et al.[41] and Goldsmith et al.[39] respectively. The hydroxy-alkenyl peroxy ($R\dot{O}_2$) radicals formed can further undergo internal H-atom shifts and further discussed in Section 3.5. The rate coefficient for reactions involving α-hydroxyalkyl radicals with O_2 to form an unsaturated aldehyde and an $H\dot{O}_2$ radical is taken from that calculated by da Silva et al.[23] for the α-hydroxyethyl + $\dot{O}_2$ reaction. Since the α site in prenol has both the character of an alpha site in an alcohol and an allylic site in an alkene, theoretical calculations are needed to explore the reaction of $\dot{O}_2$ with this unique α prenol radical.

3.5 $R\dot{O}_2$ radical isomerization to $\dot{Q}OOH$: An important step in the low-temperature radical chain branching process is the intramolecular H-atom shift of hydroxy-alkenyl peroxy ($R\dot{O}_2$) radicals to form hydroxy-alkenyl hydroperoxy ($\dot{Q}OOH$) radicals. The rate coefficients for these reactions are taken from Chen and Bozzelli.[41, 42] Reactions considered also include the β-$R\dot{O}_2$ radical undergoing Waddington decomposition via a six-membered ring isomerization

by abstracting a H-atom from the ȮH moiety. ȮOOH radicals decompose to form alkenes, aldehydes, or ketenes and an ȮH radical or an enol and HȮ$_2$ radicals. The analogous rate coefficients for the second addition of ȮOOH radicals to O_2 and the following dissociation reactions (forming carbonyl-hydroperoxides and ȮH radicals) are adopted from the work of Chen and Bozzelli[41] for the case of iso-butenyl allylic radicals.

3.6 RȮ$_2$ concerted elimination: The concerted elimination of HȮ$_2$ from RȮ$_2$ is chain propagating and competes with RȮ$_2$ radical isomerization that leads to low temperature chain branching. This elimination reaction inhibits reactivity and is a major HȮ$_2$ radical producing channel in the temperature range (600 – 1200 K). The rate coefficients for these reactions are taken from De Bruycker et al.[14]

3.7 Vinylic radical addition reactions: The presence of a C=C double bond allows for the addition of radicals such as Ḣ, ȮH, and HȮ$_2$. In the low-to-intermediate temperature regime, ȮH radical adds to the double bond, producing di-hydroxy alkyl radicals that can then add to O_2 to form di-hydroxy alkyl-peroxy radicals. The resulting RȮ$_2$ radicals can react through the Waddington mechanism, which involves an internal H-atom transfer from the hydroxyl site, followed by decomposition into an unsaturated aldehyde, ketone and an ȮH radical. Mohamed et al.[33] computed the rate coefficients for ȮH addition to prenol and these rates are used here. Ḣ atom addition to the double bond and other associated chemically activated pathways were adopted by analogy with 2-butene by Li et al.[24] and the rate coefficients for HȮ$_2$ addition were adopted from Zádor et al.[34]

4. Results and Discussion

4.1 Model validation with experimental data from this study

Figure 2 shows the IDTs for prenol/'air' mixtures measured using both the NUIG HPST and the RCM at φ = 0.5, 1.0 and 2.0, p = 15 and 30 bar. According to the experimental results,

prenol exhibits little reactivity at low temperatures and no negative temperature coefficient (NTC) behavior is observed. However, a change in slope in the ignition delay measurements can be seen at 850 – 900 K for φ = 2 at 30 bar, Fig. 2(b).

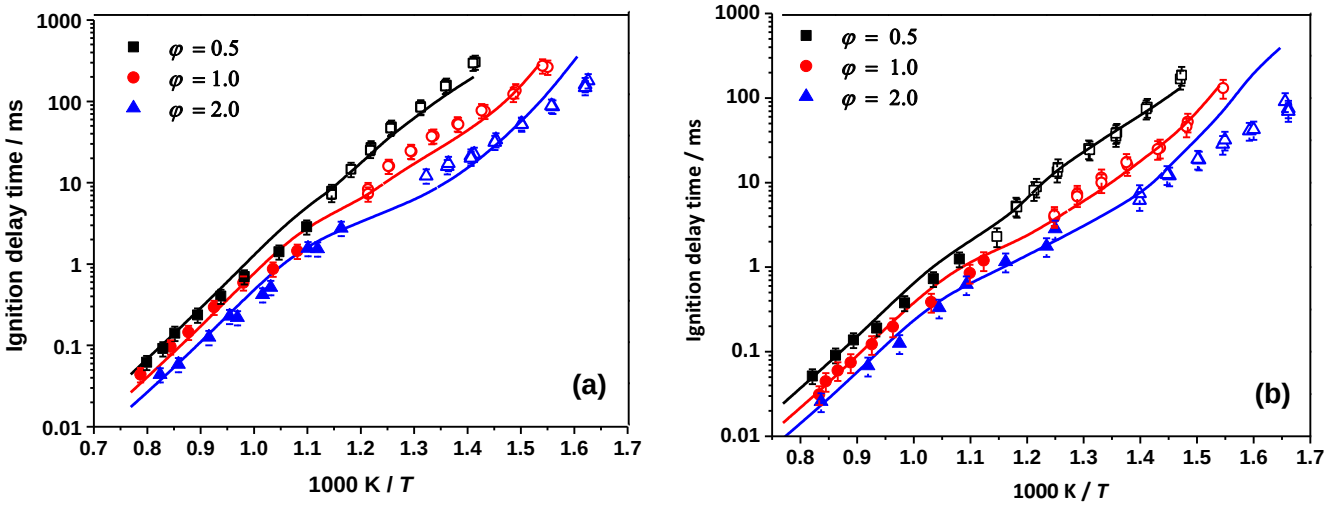

Figure 2: Experimental and simulated IDTs for prenol oxidation in air at φ = 0.5, 1.0 and 2.0, (a) p = 15 bar and (b) 30 bar. Solid symbols: HPST results, open symbols: RCM results and lines represent corresponding simulations using the current model.

These IDTs were simulated using the kinetic model developed in this work with the Chemkin Pro software[43] and ZeroRK.[44, 45] The ignition event in the simulations is defined as the time of maximum pressure rise due to ignition. For the HPST measurements, the simulations assume constant volume conditions, while for RCM measurements volume/time histories from non-reactive experiments in which the O_2 content is replaced with N_2 were used in our simulations to account for effects of the compression stroke and heat losses after compression. These volume histories are available as Supplementary material. The predictions of the current model are in excellent agreement with the measured IDTs over the entire temperature range of 600 – 1400 K for the fuel-lean and stoichiometric mixtures but are too slow (by a factor of 2) at lower temperatures for the fuel-rich mixtures below 625 K. Additional IDT validation plots

of the current model for prenol from Ninnemann et al.[13] are provided as Supplementary Material.

4.2 Reaction pathway and sensitivity analyses

Additional studies of prenol may be motivated and benefit from an understanding of the reaction pathways contributing to and controlling prenol autoignition based on the current kinetic model. Given that the current simulations capture the measured IDT well for fuel-lean and stoichiometric mixtures, two fuel-rich mixtures were selected for further analysis and discussion. The discrepancy between the simulations and experiments is largest at 30 bar and at low temperatures. Reaction flux analyses, shown in Fig. 3, from two simulations are used to discuss the low temperature autoignition chemistry at 615 K and intermediate temperature autoignition chemistry at 915 K for these fuel-rich prenol/air mixtures. These highlight the important reaction pathways controlling prenol oxidation at the time of 20% fuel consumed. The contributions of the reaction pathways at T = 615 and 915 K are presented as black and red numbers, respectively. The flux for H-atom abstraction from the allylic α-site to produce b$\dot{C}_5H_8$dj-dOH radicals at both temperatures is similar at 28%. However, H-atom abstraction from the primary allylic δ-site (to produce a$\dot{C}_5H_8$-dOH-c radicals) increases with temperature from 20% to 37%. At 615 K, a large fraction of a$\dot{C}_5H_8$-dOH-c radicals (~65%) proceed via addition to molecular oxygen forming hydroxy alkyl-peroxy radicals (R$\dot{O}_2$), which later isomerize to form $\dot{Q}$OOH radicals and decompose to aldehydic species and $\dot{O}$H radicals. At 615 K, a minor flux (~20% and hence not highlighted in the flux diagram) of allylic a$\dot{C}_5H_8$-dOH-c radicals react with H$\dot{O}_2$ radicals to form a hydroperoxide adduct which ultimately dissociates to alkoxy and $\dot{O}$H radicals, due to cleavage of the weak O–O bond. However, at 915 K, 100% of a$\dot{C}_5H_8$-dOH-c radicals preferentially undergo β-scission of the C–O bond to form isoprene (2-methyl-1,3-butadiene) and $\dot{O}$H radicals, as β-scission of the vinylic C–C is expected to be slow at these temperatures.[14] The aforementioned C–O decomposition channel

is the main formation route of isoprene, an important intermediate formed during decomposition of prenol. The α-hydroxy alkyl radical, bĊ$_5$H$_8$dj-dOH, reacts with molecular oxygen to form an unsaturated aldehyde, iC$_5$D2Y4 (prenal, or 3-methyl-2-butenal) and HȮ$_2$ radicals[23], which is the dominant pathway at both temperatures. As is the case for prenol, iC$_5$D2Y4 also undergoes H-atom abstraction reactions from the α-allylic position and from the primary allylic position to produce iC$_5$D2Y4-1j and iC$_5$D2Y4-4j radicals respectively, which ultimately produce 2-methyl-1-propenyl radicals (iĊ$_4$H$_7$-i1) and 2-methyl-acrolein (iC$_3$H$_5$CHO), respectively.

Hydroxyl radicals (ȮH) add to the double bond at both the β and γ positions, to produce Ċ$_5$H$_9$-cdOHbj and Ċ$_5$H$_9$-bdOHcj radicals, respectively, with addition to the β-site favoured at both 615 and 915 K. However, the flux via addition to the β-site decreases (by about a factor of two to three) with increasing temperature as other pathways, such as H-atom abstraction from the allylic site, become feasible. These radicals (Ċ$_5$H$_9$-cdOHbj, Ċ$_5$H$_9$-bdOHcj) further add to O$_2$ to produce C$_5$H$_9$-cdOHbȮ$_2$ and C$_5$H$_9$-cdOHcȮ$_2$ adducts, which can react through the Waddington mechanism.[46] Other minor channels (~5%) include HȮ$_2$ radical addition on the C=C bond forming an adduct, a hydroxy-hydroperoxyl alkyl radical, which promptly decomposes to form a 3-membered ring cyclic ether (3,3-dimethyl-2-methanol-oxirane) and ȮH radicals.

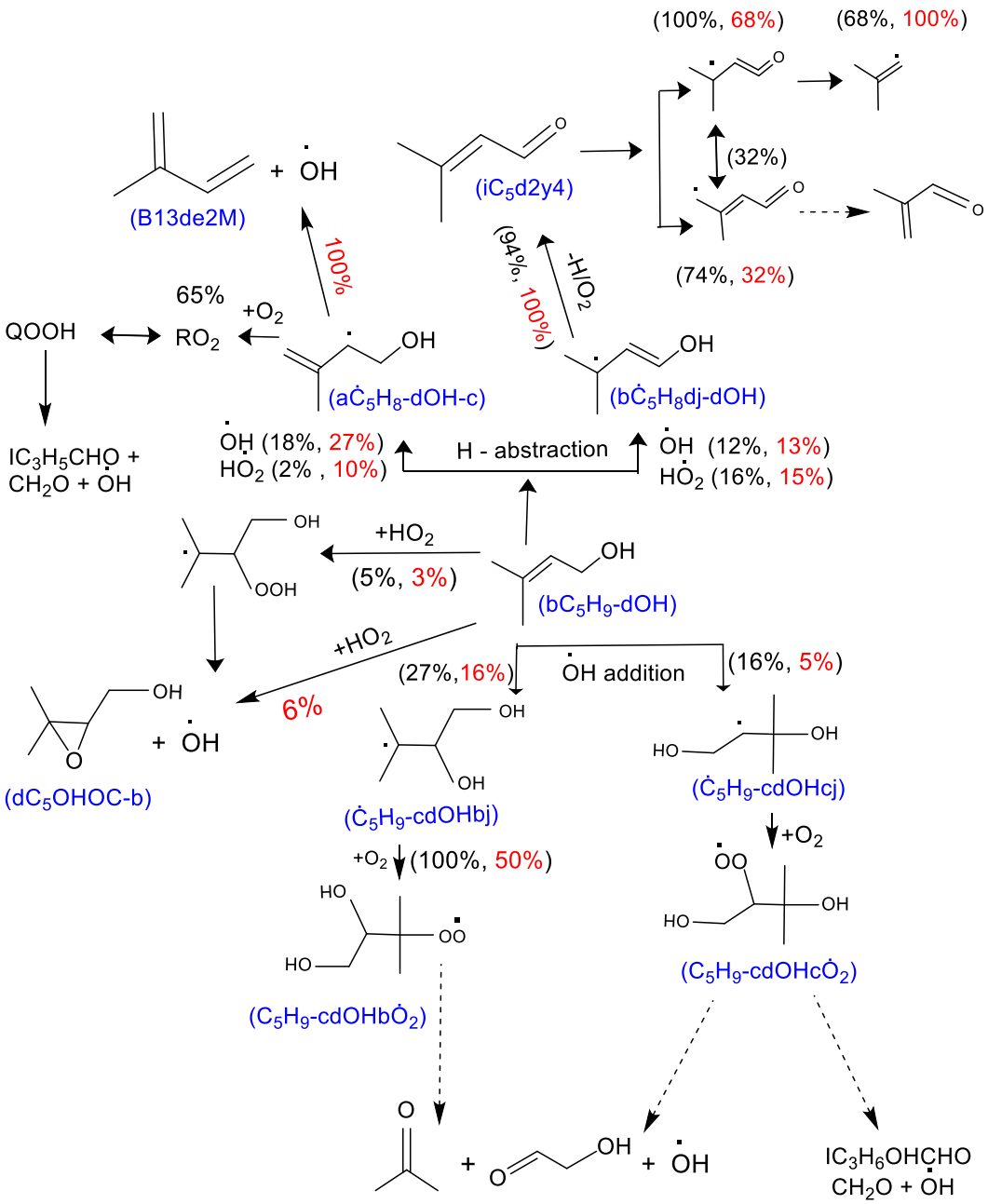

Figure 3. Flux analyses for a prenol/'air' mixture at φ = 2.0 and at p = 30 atm and 20% fuel consumption. Numbers represent the molar consumption yields expressed in relative amounts. Black numbers represent flux at 615 K and red numbers flux at 915 K.

A brute-force sensitivity analysis was performed for the auto-ignition of a prenol/air mixture at φ = 2.0, p = 30 bar, T = 615 and 915 K, and the top ten most sensitive reactions are shown in Figure 4. In the analysis, the rate coefficients of all elementary reactions were

increased and decreased by a factor of two (k^+ and k^-), and the corresponding simulations were performed adopting these changes to obtain the IDTs (τ^+ and τ^-). Following the definition above, a reaction with a positive sensitivity coefficient inhibits reactivity and vice-versa. Since the reactions are perturbed in both directions, it is important to note that the reverse direction can be the source of the observed sensitivity. This is the case for one of the sensitivities observed for low temperature reactions discussed next.

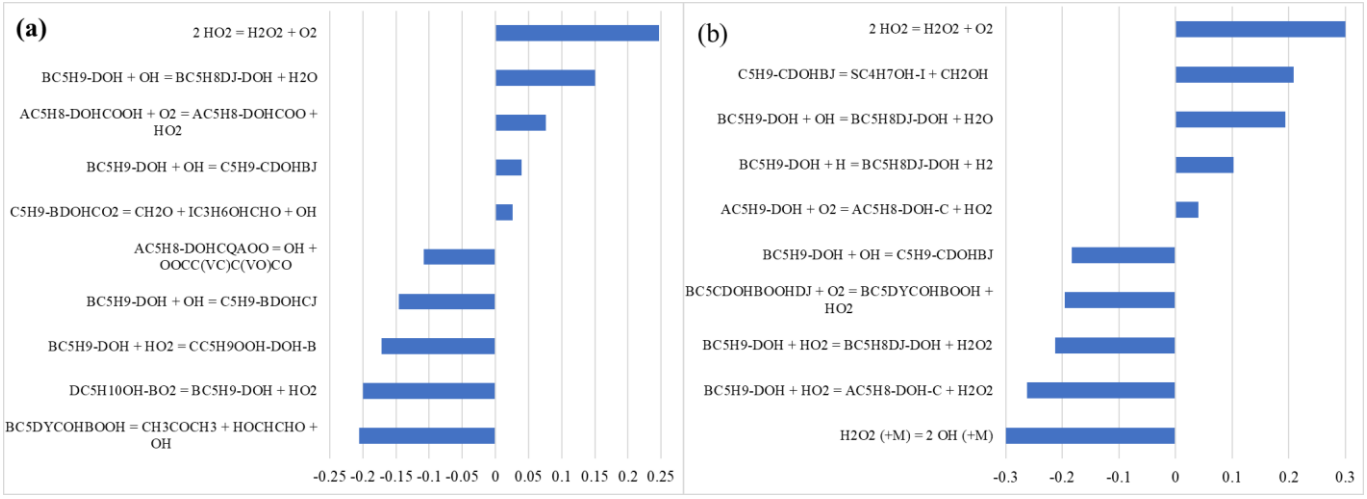

Figure 4: Reaction sensitivity to prenol IDTs at $\varphi = 2.0$ in 'air', $p = 30$ bar, (a) $T = 615$ K and (b) $T = 915$ K.

At 615 K in Fig. 4(a), the most sensitive reaction that promotes reactivity is the dissociation of the hydroxy-keto-hydroperoxide (bC$_5$dyCOHbOOH) to CH_3COCH_3 + ȮH + HOĊHCHO. Other highlighted reactions are known to be important radical consuming reactions at low-temperatures in olefins: the addition of hydroxyl and hydroperoxyl radicals to the C=C. As noted by Zador et al.[34] for a series of olefins, HȮ$_2$ addition to carbon-carbon double bonds favors the formation of alkyl-peroxy (RȮ$_2$) radicals at lower temperatures. Zador et al.[34] also note that the barrier heights of the reactions leading to hydroperoxyalkyl (ĊOOH) radicals are only slightly higher than the RȮ$_2$ pathways from olefin + HȮ$_2$. This typically leads to competitive rate coefficients at temperatures of 500 – 700 K for these two pathways which directly form RȮ$_2$ and ĊOOH. In the current model, a pathway to RȮ$_2$

formation from prenol is the reverse step of the reaction $dC_5H_{10}OH\text{-}b\dot{O}_2 = bC_5H_9\text{-}dOH + H\dot{O}_2$ listed in Fig. 4(a). These reactions are typically written as concerted eliminations in kinetic models, i.e., $R\dot{O}_2$ = olefin + $H\dot{O}_2$, and inhibit reactivity when the net flux is in the forward direction. However, allylic alpha radicals are generated from prenol which can react with oxygen to easily produce prenal and $H\dot{O}_2$, assisting formation of $R\dot{O}_2$ from prenol + $H\dot{O}_2$ at low temperatures. These $H\dot{O}_2$ additions connect to the low temperature chemistry species ($R\dot{O}_2$, $\dot{Q}OOH$) and reactions of iso-pentanol. The resulting $R\dot{O}_2$ ($dC_5H_{10}OH\text{-}b\dot{O}_2$) and $\dot{Q}OOH$ ($cC_5H_9OOH\text{-}dOH\text{-}b$) species can then proceed through conventional low temperature chemistry chain branching pathways which promote reactivity as shown in Fig. 4(a).

Several of the highly sensitive reactions shown in Fig. 4(a) are closely related to $\dot{O}H$ addition to the β and γ carbon. The $\dot{O}H$ addition to the γ-site produces $\dot{C}_5H_9\text{-}bdOHcj$ which adds O_2 to form an $R\dot{O}_2$-β species and then undergoes Waddington decomposition. The reaction sequence eventually produces one $\dot{O}H$ for one $\dot{O}H$ addition (consumption). This sequence is relatively inhibiting to ignition by competing for, and temporarily removing, $\dot{O}H$ from the radical pool and the sensitivity analysis shown in Fig. 4(a) reflects this.

However, in the case of $\dot{O}H$ addition to the β-site producing $\dot{C}_5H_9\text{-}cdOHbj$, several pathways are potentially viable. After subsequent O_2 addition at the γ carbon, the resulting $R\dot{O}_2$-γ species can undergo three distinct six- or seven-membered H-shifts. One of these isomerization reactions is also a Waddington decomposition involving the hydroxyl group at the β position. As previously discussed for the Waddington decompositions of the $R\dot{O}_2$-β isomer, the net sequence is relatively inhibiting as it returns one $\dot{O}H$ for one consumed $\dot{O}H$. A seven-membered $R\dot{O}_2$-γ isomerization with the α hydroxyl is also possible. This isomerization likely has a similar barrier height to the 1,5 Waddington decomposition. However, such 1,6 shifts are expected to have lower A-factors due to the loss of an additional rotor and is less important. A third pathway leads to a relatively novel radical branching sequence, illustrated

in Fig. 5. After ȮH addition at the β carbon and O_2 addition at the γ carbon, the fourth species (Q̇OOH) in Fig. 5 can be formed via a 1,5 H-shift from the α-site. The resulting Q̇OOH radical can then react with O_2 forming a hydroxyketohydroperoxide and $HȮ_2$ analogous to α-hydroxy alkyl radicals which form an aldehyde and $HȮ_2$. Then the hydroxyketohydroperoxide further decomposes into two radicals (ȮH, HOĊHCHO) and acetone. As three radicals (ȮH, $HȮ_2$, HOĊHCHO) are ultimately generated, the entire sequence promotes ignition. However, the effectiveness of the generated radicals to promote ignition is diminished when compared to the chain branching products of conventional low temperature chemistry (e.g., two reactive ȮH and a ketoxy radical). Therefore, this sequence does not result in negative temperature coefficient behavior.

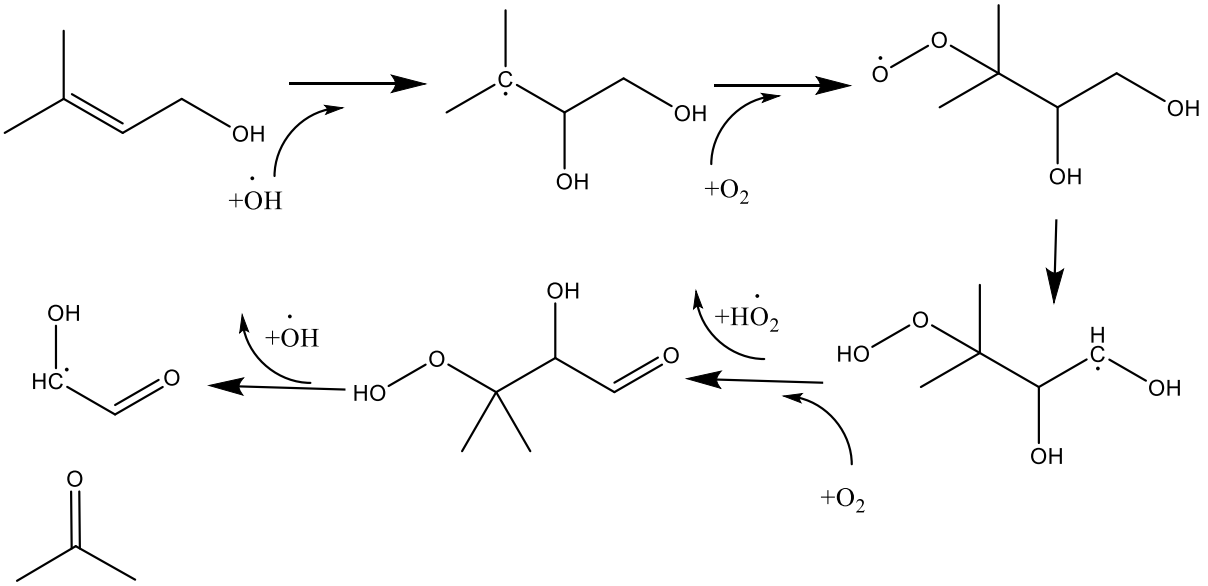

Figure 5: Low temperature reactions that lead to radical branching in prenol following ȮH addition to the β carbon. This radical branching sequence directly produces one ȮH, one $HȮ_2$, and one ketohydroxyl radical (HOĊHCHO) and does less to promote ignition than chain branching products from hydrocarbons with long alkyl chains.

At T = 915 K (Fig. 4b), the most sensitive reaction is the decomposition of H_2O_2 into two ȮH radicals, which significantly promotes the reactivity. The H-atom abstraction

reactions from fuel involving $H\dot{O}_2$ also promote reactivity since they produce H_2O_2 that decomposes into ȮH radicals at this condition. The self-recombination of $H\dot{O}_2$ radicals is a chain termination reaction, which inhibits reactivity at these conditions since it consumes two reactive radicals to form H_2O_2 and O_2 molecules. With increasing temperature, β-scission reactions become more important. At 915 K, the adduct di-hydroxy alkyl radical ($\dot{C}_5H_9$-bdOHcj) decomposes to sC_4H_7OH-i + $\dot{C}H_2OH$, which proceeds via addition to O_2 at 615 K. However, H-atom abstraction reactions from prenol by ȮH, Ḣ atoms inhibit reactivity at both temperatures, as these reactions involve the conversion of reactive radicals to less reactive prenol radicals.

4.3 Model performance against experimental data in literature

The prenol model developed in this study has been validated against the available experimental data in literature. The experimental species mole-fraction profiles obtained from the work of De Bruycker et al.[14] along with the current model predictions for the representative compounds are depicted for pyrolysis in Fig. 6 and oxidation in Fig. 7 as a function of temperature. Additional comparisons for lean mixtures are provided in the Supplementary Material (Fig. S1). The speciation experimental data provides further insight into the low temperature oxidation chemistry of prenol, and the current model can reasonably reproduce the behaviour of the experimental measurements over wide range of pyrolysis and oxidation conditions. The fuel (prenol) mole fraction profiles are well predicted by the model indicating that the rate of fuel consumption and its total reactivity was adequately considered during the mechanism development.

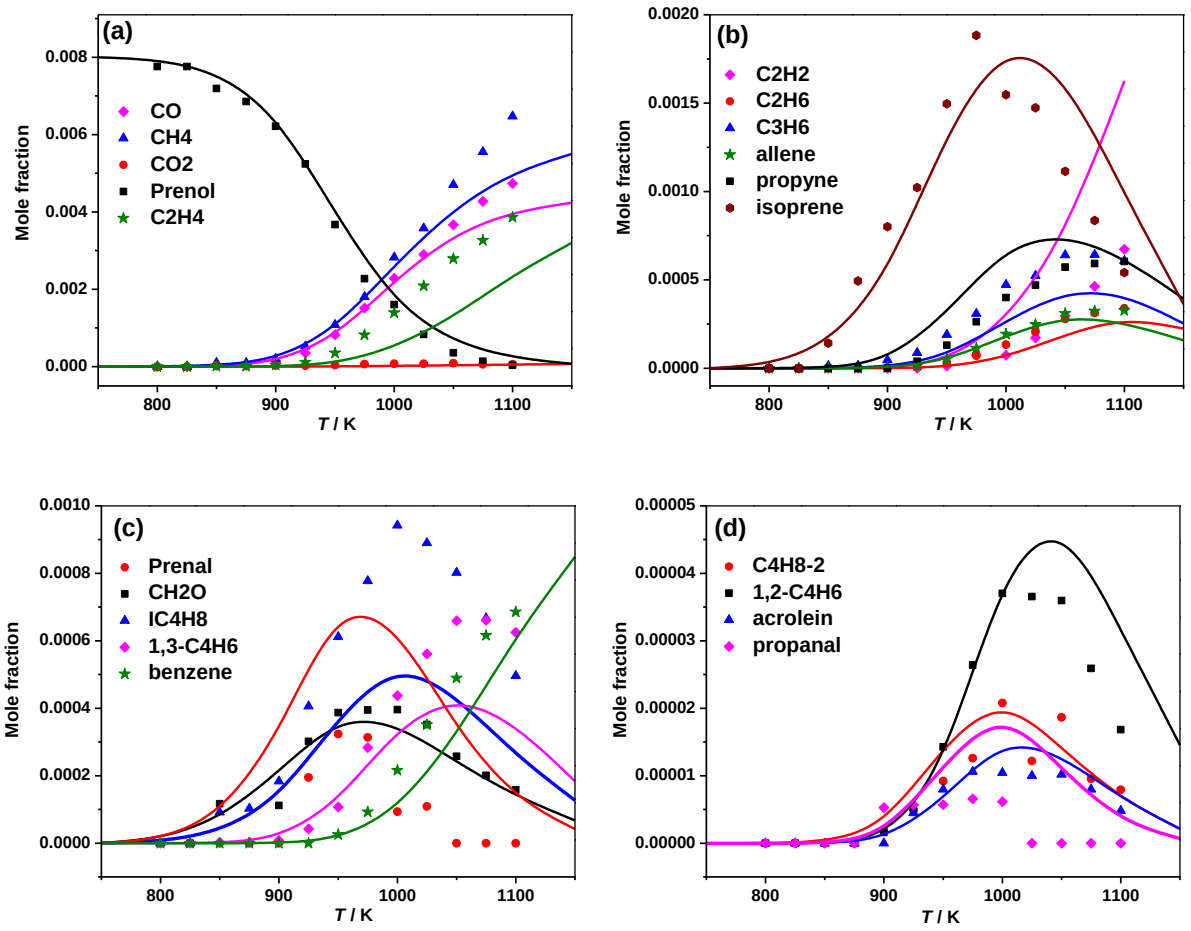

Figure 6: Species mole fraction profiles as a function of temperature for prenol pyrolysis at *p* = 1.07 bar, τ = 2 s, and mole fractions of prenol = 0.008 and He = 0.992. Points are the experimental results from De Bruycker et al.[14] and lines represent current prenol model simulations.

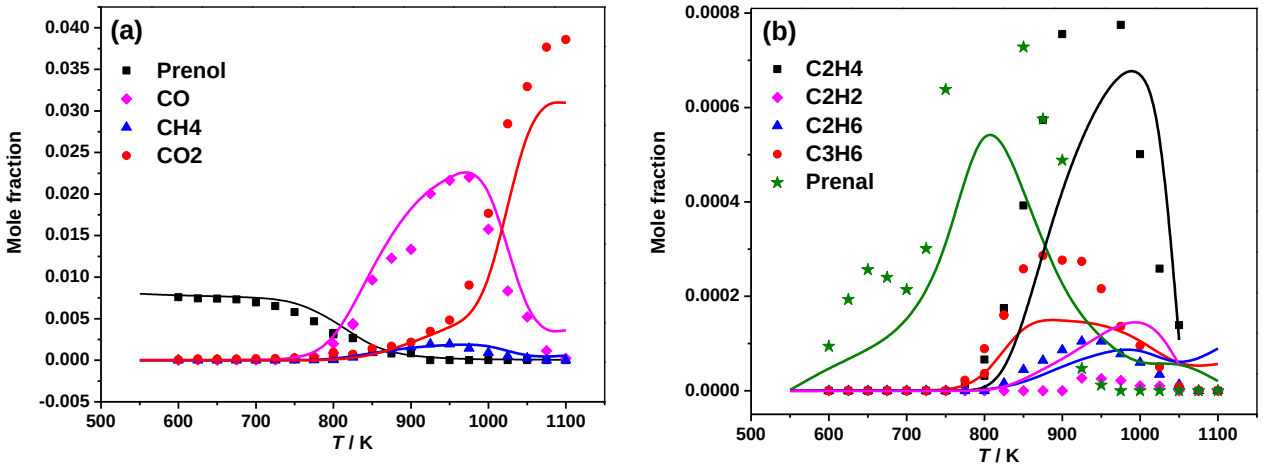

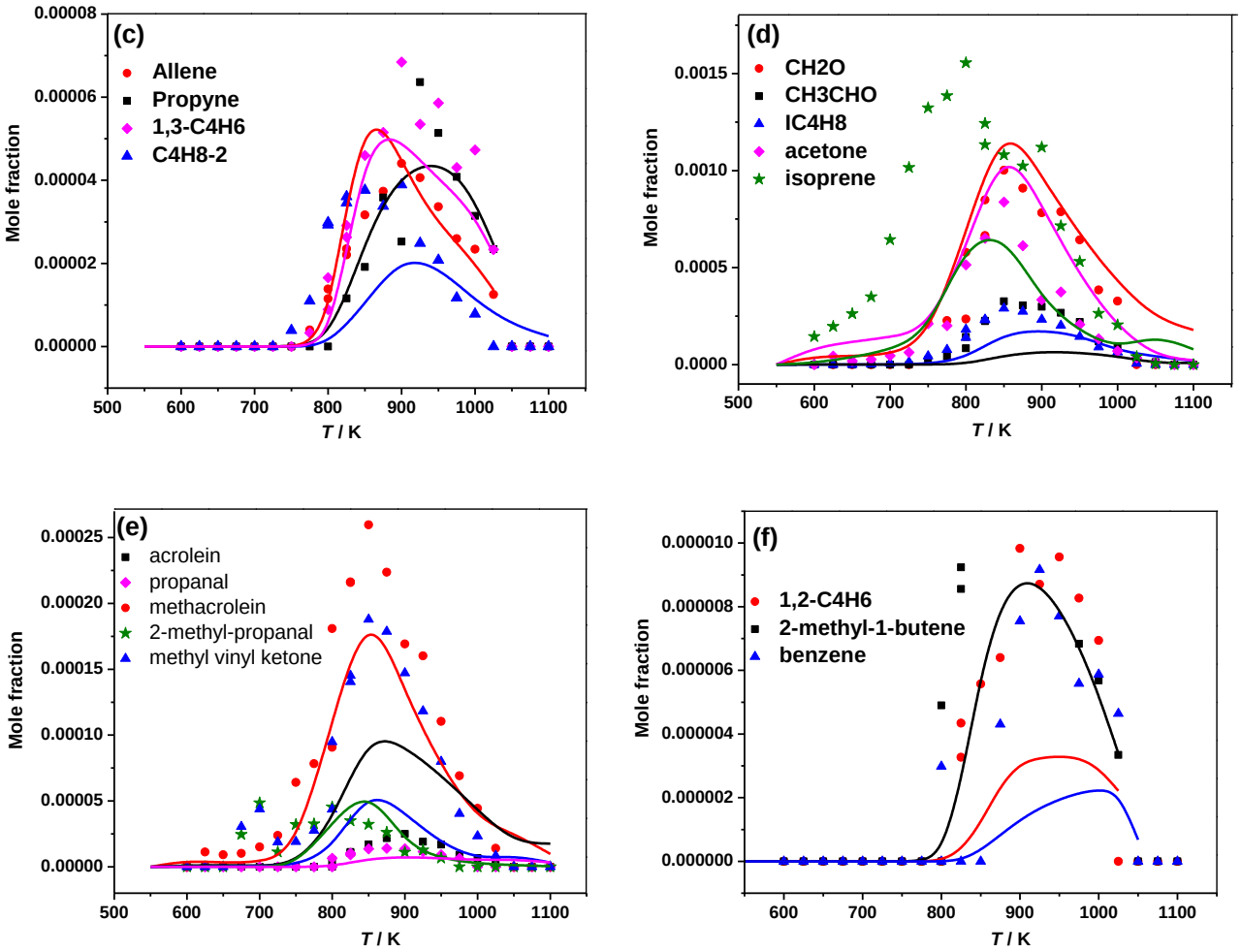

Figure 7: Species mole fraction profiles as a function of temperature for prenol oxidation at p = 1.07 bar, τ = 2 s, and φ = 1.0 prenol in air. Points are the experimental results from De Bruycker et al.[14] and lines represent current prenol model simulations.

The model can well predict isoprene mole fraction profiles at pyrolysis conditions (Fig. 6(b)) while in the presence of oxygen at φ = 1.0 (Fig. 7(d)), the predictions are underestimated by a factor of 2.5. In the case of prenal (3-methyl-2-butenal), as shown 7(b), the oxidation mole-fraction profiles, are reproduced by the model, within 20%, whereas the pyrolysis mole-fraction profiles are overestimated by a factor of two at its peak (T = 950 K), shown in Fig. 6(c). The reported experimental uncertainty is ± 15%. For other stable species measured, the current model can well reproduce the behaviour with simulations typically within a factor of two of the experimental measurements over wide range of oxidation and pyrolysis conditions.

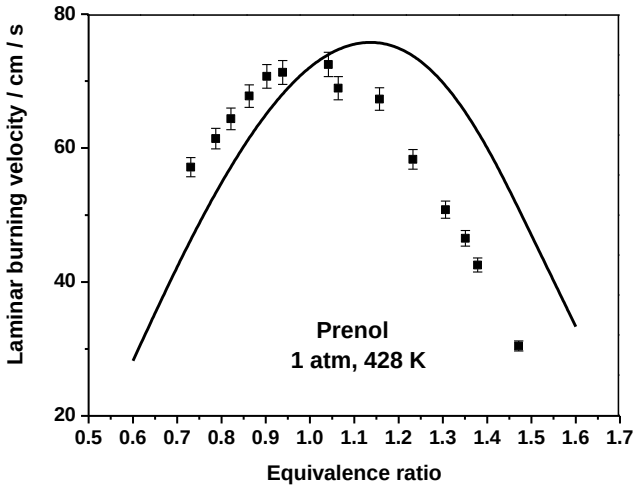

Figure 8: Laminar burning velocities of prenol as function of equivalence ratio at 1 atm and 428 K initial conditions. Points are the experimental results from Ninnemann et al.[13] and a line represents the current prenol model simulations.

Laminar burning velocities (LBV) of prenol at p = 1 atm, T = 428 K at equivalence ratios (φ) in the range 0.7 – 1.5 were reported by Ninnemann et al.[13] and these were simulated using the current model, Fig. 8. It can be observed that the predicted LBVs are shifted to higher equivalence ratios compared to the experiments where the peak value is 72 cm/s at φ = 1.03, whereas the model predicts a peak value of 76 cm/s at φ = 1.1. Due to the non-existence of a wide range of literature experimental data, there remains an outstanding question on the discrepancy of LBV agreement for prenol. Future experimental investigations of laminar flame speeds are warranted to resolve these issues, as these data are widely used to validate the predictions of kinetic models.

5. Conclusions

The oxidation of prenol/air mixtures was investigated experimentally by measuring IDTs in both a HPST and an RCM. The experimental data also provide important insights into reactivity trends in terms of temperature, pressure, and equivalence ratio. A kinetic model has

been developed which can accurately reproduce the observed autoignition behavior. The current model performance against the literature species profiles at pyrolysis and oxidation conditions over the temperature range of 600 – 1200 K is acceptable. However, discrepancies are noted in the case of experimental and calculated LBVs of prenol.

The following conclusions and recommendations are made by this study:

1. ȮH addition to the carbon-carbon double bond and subsequent reactions significantly affect the low temperature reactivity of prenol. Further studies of these pathways, as well as $H\dot{O}_2$ addition pathways, are warranted to better understand and predict the low temperature autoignition of unsaturated alcohols such as prenol.

2. The branched, unsaturated, and alcohol like features of prenol significantly hinder conventional low temperature chemistry pathways. A consequence of the structural diversity in prenol is allylic α and δ radicals generated after H-abstraction which leads to the relative inhibition and promotion of autoignition, respectively. Studies of these allylic radicals + O_2 and related pathways would be beneficial in developing rate rules for prenol and other potential biofuels which may produce allylic radicals with similar characteristics.

3. Major intermediates such as prenal (3-methyl-2-butenal) and isoprene (2-methyl-1,3-butadiene) formed during the pyrolysis and oxidation of prenol are not well studied. Future work focused on the combustion chemistry of these significant intermediates is warranted.

Supporting Information

- A word document containing additional literature validations and ignition delay time correlations
- A zip folder containing three text files in CHEMKIN format describing: kinetics, thermodynamic properties, and transport properties
- A worksheet containing the new ignition delay time measurements from this study

- Volume histories for simulations of the rapid compression machine experiments

Declaration of competing interest

None.

Acknowledgments

The authors at NUI Galway recognize funding support from Science Foundation Ireland through project number 15/IA/3177. The work at LLNL was performed under the auspices of the U.S. Department of Energy (DOE) by Lawrence Livermore National Laboratory under Contract DE-AC52-07NA27344 and was conducted as part of the Co-Optimization of Fuels & Engines (Co-Optima) project sponsored by the DOE Office of Energy Efficiency and Renewable Energy (EERE), Bioenergy Technologies and Vehicle Technologies Offices.

References:

1. Kalghatgi, G. T., Fuel Anti-Knock Quality - Part I. Engine Studies. *SAE Transactions* **2001,** 110, 1993-2004.
2. Demirbas, A., Progress and recent trends in biofuels. *Prog. Energy Combust. Sci.* **2007,** 33(1), 1-18.
3. Hansen, A. C.; Zhang, Q.; Lyne, P. W. L., Ethanol–diesel fuel blends — a review. *Bioresour. Technol.* **2005,** 96(3), 277-285.
4. Mack, J. H.; Rapp, V. H.; Broeckelmann, M.; Lee, T. S.; Dibble, R. W., Investigation of biofuels from microorganism metabolism for use as anti-knock additives. *Fuel* **2014,** 117, 939-943.
5. Farrell, J. T.; Holladay, J.; Wagner, R., Fuel Blendstocks with the Potential to Optimize Future Gasoline Engine Performance: Identification of Five Chemical Families for Detailed Evaluation. *Technical Report. U.S. Department of Energy, Washington, DC. 2018. DOE/GO-102018-4970.*
6. Wang, Z.; Liu, H.; Reitz, R. D., Knocking combustion in spark-ignition engines. *Prog. Energy Combust. Sci.* **2017,** 61, 78-112.
7. Gaspar, D. J.; West, B. H.; Ruddy, D.; Wilke, T. J.; Polikarpov, E.; Alleman, T. L.; George, A.; Monroe, E.; Davis, R. W.; Vardon, D.; Sutton, A. D.; Moore, C. M.; Benavides, P. T.; Dunn, J.; Biddy, M. J.; Jones, S. B.; Kass, M. D.; Pihl, J. A.; Pihl, J. A.; Debusk, M. M.; Sjoberg, M.; Szybist, J.; Sluder, C. S.; Fioroni, G.; Pitz, W. J., Top Ten Blendstocks Derived From Biomass For Turbocharged Spark Ignition Engines: Bio-blendstocks With Potential for Highest Engine Efficiency. . **2019**.
8. Monroe, E.; Gladden, J.; Albrecht, K. O.; Bays, J. T.; McCormick, R.; Davis, R. W.; George, A., Discovery of novel octane hyperboosting phenomenon in prenol biofuel/gasoline blends. *Fuel* **2019,** 239, 1143-1148.
9. Zheng, Y.; Liu, Q.; Li, L.; Qin, W.; Yang, J.; Zhang, H.; Jiang, X.; Cheng, T.; Liu, W.; Xu, X.; Xian, M., Metabolic engineering of Escherichia coli for high-specificity production of isoprenol and prenol as next generation of biofuels. *Biotechnol. Biofuels.* **2013,** 6(1), 57.
10. Atsumi, S.; Hanai, T.; Liao, J. C., Non-fermentative pathways for synthesis of branched-chain higher alcohols as biofuels. *Nature* **2008,** 451(7174), 86-89.

11. Chou, H. H.; Keasling, J. D., Synthetic Pathway for Production of Five-Carbon Alcohols from Isopentenyl Diphosphate. *Appl. Environ. Microbiol.* **2012,** 78(22), 7849.
12. George, K. W.; Thompson, M. G.; Kang, A.; Baidoo, E.; Wang, G.; Chan, L. J. G.; Adams, P. D.; Petzold, C. J.; Keasling, J. D.; Soon Lee, T., Metabolic engineering for the high-yield production of isoprenoid-based C5 alcohols in E. coli. *Sci. Rep.* **2015,** 5(1), 11128.
13. Ninnemann, E.; Kim, G.; Laich, A.; Almansour, B.; Terracciano, A. C.; Park, S.; Thurmond, K.; Neupane, S.; Wagnon, S.; Pitz, W. J.; Vasu, S. S., Co-optima fuels combustion: A comprehensive experimental investigation of prenol isomers. *Fuel* **2019,** 254, 115630.
14. De Bruycker, R.; Herbinet, O.; Carstensen, H.-H.; Battin-Leclerc, F.; Van Geem, K. M., Understanding the reactivity of unsaturated alcohols: Experimental and kinetic modeling study of the pyrolysis and oxidation of 3-methyl-2-butenol and 3-methyl-3-butenol. *Combust. Flame.* **2016,** 171, 237-251.
15. Vandewiele, N. M.; Van Geem, K. M.; Reyniers, M.-F.; Marin, G. B., Genesys: Kinetic model construction using chemo-informatics. *Chem. Eng. J.* **2012,** 207-208, 526-538.
16. Nakamura, H.; Darcy, D.; Mehl, M.; Tobin, C. J.; Metcalfe, W. K.; Pitz, W. J.; Westbrook, C. K.; Curran, H. J., An experimental and modeling study of shock tube and rapid compression machine ignition of n-butylbenzene/air mixtures. *Combust. Flame.* **2014,** 161(1), 49-64.
17. Gallagher, S. M.; Curran, H. J.; Metcalfe, W. K.; Healy, D.; Simmie, J. M.; Bourque, G., A rapid compression machine study of the oxidation of propane in the negative temperature coefficient regime. *Combust. Flame.* **2008,** 153(1), 316-333.
18. Morley, C., Gaseq, http:www.gaseq.co.uk.
19. Petersen, E. L.; Rickard, M. J. A.; Crofton, M. W.; Abbey, E. D.; Traum, M. J.; Kalitan, D. M., A facility for gas- and condensed-phase measurements behind shock waves. *Measurement Science and Technology* **2005,** 16(9), 1716-1729.
20. Baigmohammadi, M.; Patel, V.; Martinez, S.; Panigrahy, S.; Ramalingam, A.; Burke, U.; Somers, K. P.; Heufer, K. A.; Pekalski, A.; Curran, H. J., A Comprehensive Experimental and Simulation Study of Ignition Delay Time Characteristics of Single Fuel C1–C2 Hydrocarbons over a Wide Range of Temperatures, Pressures, Equivalence Ratios, and Dilutions. *Energy & Fuels* **2020,** 34(3), 3755-3771.
21. Lee, D.; Hochgreb, S., Rapid Compression Machines: Heat Transfer and Suppression of Corner Vortex. *Combust. Flame.* **1998,** 114(3), 531-545.
22. Sarathy, S. M.; Oßwald, P.; Hansen, N.; Kohse-Höinghaus, K., Alcohol combustion chemistry. *Prog. Energy Combust. Sci.* **2014,** 44, 40-102.
23. da Silva, G.; Bozzelli, J. W.; Liang, L.; Farrell, J. T., Ethanol Oxidation: Kinetics of the α-Hydroxyethyl Radical + O2 Reaction. *J. Phys. Chem.* **2009,** 113(31), 8923-8933.
24. Li, Y.; Zhou, C.-W.; Somers, K. P.; Zhang, K.; Curran, H. J., The oxidation of 2-butene: A high pressure ignition delay, kinetic modeling study and reactivity comparison with isobutene and 1-butene. *Proc. Combust. Inst.* **2017,** 36(1), 403-411.
25. Ritter, E. R.; Bozzelli, J. W., THERM: Thermodynamic property estimation for gas phase radicals and molecules. *Int. J. Chem. Kinet.* **1991,** 23(9), 767-778.
26. Burke, S. M.; Simmie, J. M.; Curran, H. J., Critical Evaluation of Thermochemical Properties of C1–C4 Species: Updated Group-Contributions to Estimate Thermochemical Properties. *J. Phys. Chem. Ref. Data.* **2015,** 44(1), 013101.
27. Li, Y.; Curran, H. J., Extensive Theoretical Study of the Thermochemical Properties of Unsaturated Hydrocarbons and Allylic and Super-Allylic Radicals: The Development and Optimization of Group Additivity Values. *J. Phys. Chem.* **2018,** 122(20), 4736-4749.
28. Ye, L.; Georgievskii, Y.; Klippenstein, S. J., Pressure-dependent branching in the reaction of 1CH2 with C2H4 and other reactions on the C3H6 potential energy surface. *Proc. Combust. Inst.* **2015,** 35(1), 223-230.
29. Tsang, W., Chemical Kinetic Data Base for Combustion Chemistry Part V. Propene. *J. Phys. Chem. Ref. Data.* **1991,** 20(2), 221-273.

30. Tsang, W.; Hampson, R. F., Chemical Kinetic Data Base for Combustion Chemistry. Part I. Methane and Related Compounds. *J. Phys. Chem. Ref. Data.* **1986,** 15(3), 1087-1279.
31. Zhou, C.-W.; Simmie, J. M.; Somers, K. P.; Goldsmith, C. F.; Curran, H. J., Chemical Kinetics of Hydrogen Atom Abstraction from Allylic Sites by 3O2; Implications for Combustion Modeling and Simulation. *J. Phys. Chem.* **2017,** 121(9), 1890-1899.
32. Cavallotti, C.; Leonori, F.; Balucani, N.; Nevrly, V.; Bergeat, A.; Falcinelli, S.; Vanuzzo, G.; Casavecchia, P., Relevance of the Channel Leading to Formaldehyde + Triplet Ethylidene in the O(3P) + Propene Reaction under Combustion Conditions. *J. Phys. Chem. Lett.* **2014,** 5(23), 4213-4218.
33. Mohamed, S. Y.; Monge-Palacios; Giri, B. R.; Khaled, F.; Liu, D.; Farooq, A.; Sarathy, M., A Shock Tube and Multi-Structural Torsional Variational Transition State Theory Study

in review **2021**.
34. Zádor, J.; Klippenstein, S. J.; Miller, J. A., Pressure-Dependent OH Yields in Alkene + HO2 Reactions: A Theoretical Study. *J. Phys. Chem.* **2011,** 115(36), 10218-10225.
35. Lokachari, N.; Wagnon, S. W.; Kukkadapu, G.; Pitz, W. J.; Curran, H. J., An experimental and kinetic modeling study of cyclopentane and dimethyl ether blends. *Combust. Flame.* **2021,** 225, 255-271.
36. Wu, C.-W.; Lee, Y.-P.; Xu, S.; Lin, M. C., Experimental and Theoretical Studies of Rate Coefficients for the Reaction O(3P) + C2H5OH at High Temperatures. *J. Phys. Chem.* **2007,** 111(29), 6693-6703.
37. Mittal, G.; Burke, S. M.; Davies, V. A.; Parajuli, B.; Metcalfe, W. K.; Curran, H. J., Autoignition of ethanol in a rapid compression machine. *Combust. Flame.* **2014,** 161(5), 1164-1171.
38. Li, Y.; Klippenstein, S. J.; Zhou, C.-W.; Curran, H. J., Theoretical Kinetics Analysis for Ḣ Atom Addition to 1,3-Butadiene and Related Reactions on the Ċ4H7 Potential Energy Surface. *J. Phys. Chem.* **2017,** 121(40), 7433-7445.
39. Goldsmith, C. F.; Klippenstein, S. J.; Green, W. H., Theoretical rate coefficients for allyl+HO2 and allyloxy decomposition. *Proc. Combust. Inst.* **2011,** 33(1), 273-282.
40. Matheu, D. M.; Green Jr., W. H.; Grenda, J. M., Capturing pressure-dependence in automated mechanism generation: Reactions through cycloalkyl intermediates. *Int. J. Chem. Kinet.* **2003,** 35(3), 95-119.
41. Chen, C.-J.; Bozzelli, J. W., Thermochemical Property, Pathway and Kinetic Analysis on the Reactions of Allylic Isobutenyl Radical with O2: an Elementary Reaction Mechanism for Isobutene Oxidation. *J. Phys. Chem.* **2000,** 104(43), 9715-9732.
42. Sun, H.; Bozzelli, J. W.; Law, C. K., Thermochemical and Kinetic Analysis on the Reactions of O2 with Products from OH Addition to Isobutene, 2-Hydroxy-1,1-dimethylethyl, and 2-Hydroxy-2-methylpropyl Radicals: HO2 Formation from Oxidation of Neopentane, Part II. *J. Phys. Chem.* **2007,** 111(23), 4974-4986.
43. Reaction Workbench 15131, Reaction Design, San Diego. **2013**.
44. Cheng, S.; Kang, D.; Fridlyand, A.; Goldsborough, S. S.; Saggese, C.; Wagnon, S.; McNenly, M. J.; Mehl, M.; Pitz, W. J.; Vuilleumier, D., Autoignition behavior of gasoline/ethanol blends at engine-relevant conditions. *Combust. Flame.* **2020,** 216, 369-384.
45. McNenly, M. J.; Whitesides, R. A.; Flowers, D. L., Faster solvers for large kinetic mechanisms using adaptive preconditioners. *Proc. Combust. Inst.* **2015,** 35(1), 581-587.
46. Ray, D. J. M.; Ruiz Diaz, R.; Waddington, D. J., Gas-phase oxidation of butene-2: The role of acetaldehyde in the reaction. *Proc. Combust. Inst.* **1973,** 14(1), 259-266.

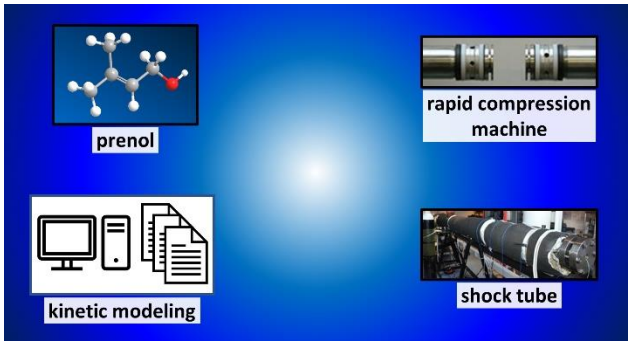
prenol
rapid compression machine
kinetic modeling
shock tube

TOC Graphic